ACS APPLIED MATERIALS & INTERFACES

Research Article

www.acsami.org

Photothermal Control of Membrane Permeability of Microcapsules for On-Demand Release

Woong-Chan Jeong,[†,‡] Shin-Hyun Kim,*[,†] and Seung-Man Yang*[,†,‡,§]

[†]Department of Chemical and Biomolecular Engineering and [‡]National Creative Research Initiative Center for Integrated Optofluidic Systems, Korea Advanced Institute of Science and Technology, 335 Gwahangno, Yuseong-gu, Daejeon 305-701, Korea

Supporting Information

ABSTRACT: We report the use of a simple microfluidic device for producing microcapsules with reversible membrane permeability that can be remotely controlled by application of near-infrared (NIR) light. Water-in-oil-in-water (W/O/W) double-emulsion drops were prepared to serve as templates for the production of mechanically stable microcapsules with a core−shell structure and highly uniform size distribution. A biocompatible ethyl cellulose shell was formed, containing densely packed thermoresponsive poly(*N*-isopropylacrylamide) (pNIPAAm) particles in which gold nanorods were embedded. Irradiation with a NIR laser resulted in heating of the hydrogel particles due to the photothermal effect of the gold nanorods, which absorb at that wavelength. This localized heating resulted in shrinkage of the particles and formation of macrogaps between them and the matrix of the membrane. Large encapsulated molecules could then pass through these gaps into the surrounding fluid. As the phase transition behavior of pNIPAAm is highly reversible, this light-triggered permeability could be repeatedly switched on and off by removing the laser irradiation for sufficient time to allow the gold nanorods to cool. This reversible and remote control of permeability enabled the programmed release of encapsulants, with the time and period of the open valve state able to be controlled by adjusting the laser exposure. This system thus has the potential for spatiotemporal release of encapsulated drugs.

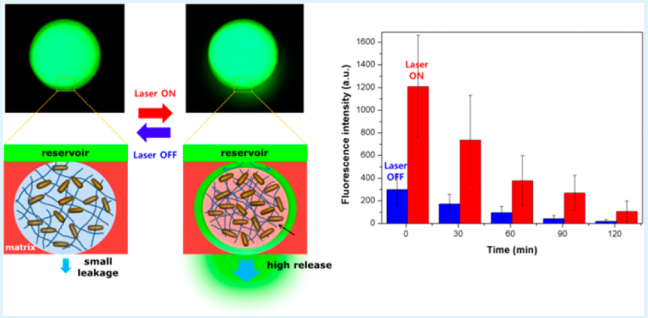

KEYWORDS: *microcapsule, microfluidics, on-demand release, photothermal effect*

INTRODUCTION

Drug delivery systems have been extensively studied for transporting pharmaceutical compounds to a desired location within the human body to achieve a therapeutic effect. One of the most important functions of drug carriers is their ability to release drugs on demand, which can reduce toxicity and enhance efficacy by controlling the time and duration of exposure to the compound. To implement such a function in microcarriers, various types of stimuli-responsive materials have been studied, along with corresponding external stimuli such as light, magnetic fields, ultrasound, and electric fields.[1−6] In particular, sets of stimuli and materials that enable the reversible and remote control of the microcarrier membrane permeability are highly promising owing to the possibility to achieve programmable release. Near-infrared (NIR) light is an important potential stimulus because it can be focused onto a small, specific area and penetrate deeply into tissue with insignificant damage. Therefore, NIR-responsive microcarriers with a function of stimulated local release of payloads will provide great potential in drug delivery applications.

To date, several types of NIR-responsive microcapsules have been developed for achieving triggered release of encapsulants. For example, Lee et al.[7] prepared microcapsules of poly(DL-lactic-*co*-glycolic acid) (PLGA) containing gold nanorods. Upon laser irradiation, the nanorods generated heat via a photothermal effect, and as a result, the membrane became more permeable above the glass transition temperature of the PLGA, thereby providing remote control release of the encapsulant. Thermoresponsive polymersomes have also been prepared for remote triggering of encapsulant release, with incorporation of gold nanoparticles in their bilayer membrane enabling light-triggered rupture.[8] Kim et al.[9] designed hydrogel capsules with membranes composed of poly(*N*-isopropylacrylamide) (pNIPAAm) containing gold nanorods and achieved reversible control of permeability. However, these polymeric or hydrogel microcapsules exhibited relatively poor mechanical properties, frequently leading to undesired rupture or deformation of the shell membrane in physiological environments. In addition, drug diffusion through the polymer matrix of the shell is limited to small molecules. Therefore, production of robust microcapsules that provide remote and reversible control of drug release, especially for high molecular weight compounds, in addition to liposome or metal nanoparticle releases, remains an important need.

Received: September 4, 2013
Accepted: December 27, 2013
Published: December 27, 2013

   dx.doi.org/10.1021/am4037993 | *ACS Appl. Mater. Interfaces* 2014, 6, 826−832

Here, we report photo- and thermoresponsive microcapsules whose porous membranes contain reversible valves. Using a cheap and simple microfluidic device, we prepared water−oil−water (W/O/W) double-emulsion drops, which served as templates to produce microcapsules. The capsule membrane, made from the middle oil phase, was designed to contain interconnected pores that could be filled by a thermoresponsive hydrogel. To provide photoresponsiveness, gold nanorods were embedded in the hydrogel matrix to act as nanoheaters under NIR irradiation. The microcapsules were demonstrated to exhibit NIR-triggered release of a model drug with high molecular weight, with the release event successfully occurring repeatedly over extended periods by a series of NIR exposures. In addition, a porous membrane made of the biocompatible polymer, ethyl cellulose, provided high mechanical stability and membrane integrity.

EXPERIMENTAL SECTION

Preparation of Microcapsules. A precursor solution was prepared, consisting of an aqueous mixture of 8 wt % *N*-isopropylacrylamide monomer (NIPAAm, Acros Organics), 1.2 wt % *N*′-methylenebisacrylamide crosslinker (BIS, Sigma-Aldrich), 1.9 wt % 2-(methacryloyloxy) ethyl trimethyl ammonium chloride (METAC, Sigma-Aldrich), 1.5 wt % ammonium persulfate (APS, Sigma-Aldrich), and 1.5 wt % gold nanorods. The METAC was added to reduce the inhomogeneity of the polymer network, which can be caused by the heat generation during polymerization.[10,11] High contents of BIS increase crosslinking density, thereby reducing water content and pore size in the swollen state; this enables us to maintain the shape of hydrogel particles during capsule fabrication and to capture gold nanorods in the gel matrix without leakage. The gold nanorods had an average width of 9 nm and length of 38 nm and were functionalized with poly(ethylene glycol) to increase their dispersion stability.[12] The absorbance peak of an aqueous suspension of the gold nanorods was at 820 nm.[13] The oil phase consisted of a mixture of dichloromethane (DCM) and hexane in a weight ratio of 7:3, containing 8 wt % ethyl cellulose. The aqueous solution of hydrogel precursors and the oil phase were mixed at a weight ratio of 1:7, and the mixture was emulsified using a high speed shear mixer and homogenizer, yielding water-in-oil (W/O) emulsion droplets with a diameter of 0.3−10 μm. To polymerize the precursors at room temperature, the initiator, *N*,*N*,*N*′,*N*′-tetramethylethylenediamine (TEMED) was dissolved in DCM at a concentration of 9 wt % and added to the emulsion to a final concentration of 1 wt % in the oil phase. As the TEMED is soluble in both oil and water, it would rapidly diffuse into the aqueous droplets and trigger free-radical copolymerization. The density of the oil phase was carefully controlled to match that of the aqueous phase (density ≈ 1.03); this causes very slow sedimentation of the aqueous emulsion drops during the polymerization process, thereby preventing their coalescence on the bottom. The polymerization was allowed to proceed in a closed vial at room temperature for 6 h, resulting in the formation of spherical hydrogel particles of pNIPAAm in the oil phase.

Fabrication of a Microfluidic Device. The microfluidic device consisted of three polypropylene pipette tips of different sizes (Eppendorf), one glass capillary with an inner diameter of 0.5 mm and outer diameter of 0.9 mm (1B100-3; World Precision Instruments, Inc.), and polyethylene (PE) tubing (BD intramedic). To fabricate the devices, the three pipette tips and glass capillary were coaxially aligned and assembled, as shown in Figures S1 and S2 of the Supporting Information. The smallest pipette tip and one of the PE tubes were inserted into the wide opening of the second pipette tip, which was cut to give a section with a 6 mm opening at one end and a 1 mm opening at the other. These tips were used for injection of the innermost and middle phases, respectively. The second tip was inserted into the wide opening of the third pipette tip, which was cut to give an opening of 5.5 mm at one end and 2.5 mm at the other. A glass capillary and some PE tubing were then inserted into the other end of this third tip. To achieve sufficient alignment, a stainless steel wire with a diameter of 0.5 mm was inserted through all orifices of the three pipette tips and the glass capillary, and then the coaxially aligned assembly was fixed and sealed with epoxy putty adhesive. Finally, the wire was removed, and PE tubing was inserted into the wide opening of the smallest pipette tip and sealed. This approach provided a simple and cheap microfluidic device for preparation of W/O/W double-emulsion drops without the need for complex surface modification and patterning. In addition, as the polymeric pipette tips were highly resistant to organic solvents, they could be used with hexane and DCM.

Preparation of Monodisperse Double-Emulsion and Ethyl Cellulose Microcapsules. To prepare the double-emulsion templates, the innermost aqueous phase, middle oil phase, and continuous aqueous phase were injected into the microfluidic device at independently controlled flow rates using three syringe pumps (KDS200, KD Scientific). An aqueous solution of 2 wt % poly(vinyl alcohol) (PVA, 87−89% hydrolyzed, M_w 13 000−23 000, Sigma-Aldrich) was used for the innermost and aqueous phases. For visualization of the release, fluorescein isothiocyanate-dextran (FITC-dextran, M_w 2 000 000, Sigma-Aldrich) was dissolved in the innermost phase at a concentration of 2 wt %, in some experiments. For the middle oil phase, the pNIPAAm particle-dispersed mixture of DCM and hexane containing 8 wt % ethyl cellulose was used. In some experiments, the hydrophobic fluorescent dye, Nile Red (Sigma-Aldrich), was added to this oil phase at a concentration of 0.005 wt % to allow clear visualization of the shell. In the microfluidic device, the three phases were coaxially injected into a single orifice of the glass capillary, forming double-emulsion drops through single-step emulsification. The inner and outer interfaces were simultaneously broken to form a drop-in-drop structure. The double-emulsion drops were collected in an aqueous solution of 0.5 wt % PVA and incubated to evaporate the volatile solvent at room temperature for approximately 3 h.

Characterization. The absorption spectrum of the gold nanorods dispersed in water was measured using a UV-visible spectrometer (UV-2450, SHIMADZU). To evaluate the photoresponsiveness of the microcapsule membranes, a NIR laser (LVI808CW4WF-VA, LVI technology) with 1 W output power at 808 nm was used; the irradiation power of 1 W ensured the complete shrinking of the hydrogel particles in water medium. To characterize the release of FITC-dextran as a model compound, a fluorescence microscope (Eclipse TE 2000-U, Nikon) was employed. Average fluorescence intensities were calculated from the images of 25 microcapsules randomly selected from each sample. Scanning electron microscopy (SEM, Hitachi, S-4800) was used to observe macropores in the membrane, and transmission electron microscopy (TEM, Hitachi, HD-2300A and TECNAI F20) was used to observe the nanorod-embedded hydrogel particles.

RESULTS

Photo- and thermoresponsive microcapsules were prepared and used for NIR-triggered release of encapsulants, as schematically illustrated in Figure 1. The ethyl cellulose membrane is stable against light, heat, and chemicals and exhibits high mechanical strength (Sward hardness of 52−61 in 3-mil. film).[14,15] The capsule shell contained pNIPAAm particles, with gold nanorods embedded in each one. The pNIPAAm exhibits a phase transition at a certain temperature; it is hydrophilic and swollen in water at temperatures below its lower critical solution temperature (LCST) while hydrophobic and deswollen at temperatures above it. Therefore, at low temperature, the pNIPAAm particle-embedded capsule membrane would not be permeable to molecules larger than the diameter of its pores. In contrast, above the LCST, the particles would become deswollen and would shrink, resulting in the formation of macroscopic gaps between the rigid ethyl cellulose membrane and the pNIPAAm particles. This would allow diffusion of relatively large molecules from the capsule interior to the

dx.doi.org/10.1021/am4037993 | ACS Appl. Mater. Interfaces 2014, 6, 826−832

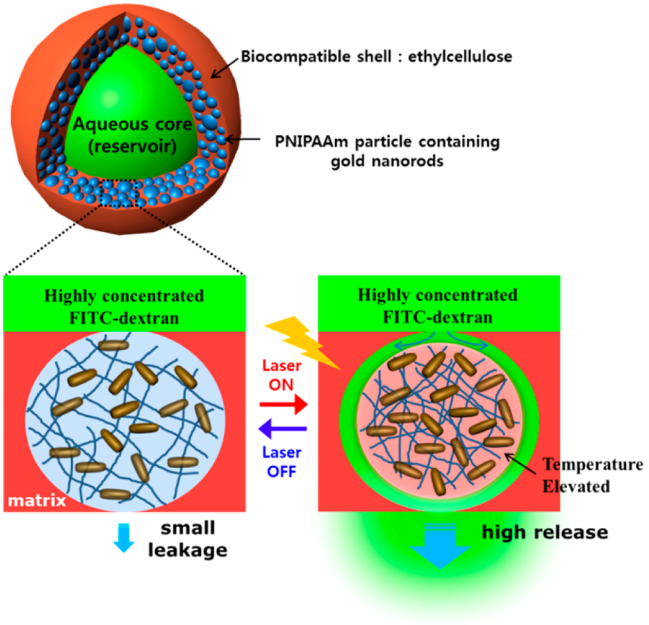

Figure 1. Schematic diagram showing the microcapsule structure and the payload release on irradiation with the NIR laser.

surrounding fluid.[16] As the phase transition of the polymer is reversible, the formation of these large gaps could be controlled by switching the temperature above and below the LCST. In the present study, gold nanorods were embedded in the particles to enable the remote switching of these states with the use of NIR light irradiation. The nanorods would absorb the NIR and then generate heat through a photothermal effect. Therefore, NIR laser irradiation would cause a local increase in temperature, thereby providing on-demand release of encapsulants. When the laser is turned off, the pNIPAAm particles are cooled by the surrounding membrane and fluids that have remained at low temperature, thereby resulting in reswelling of the particles and closure of the gaps in the membrane. This reversible control of the open/closed states of the membrane pores facilitates on-demand release of encapsulated molecules or particles that are larger than the mesh size of the hydrogel but smaller than the size of macrogaps.

The synthesized gold nanorods exhibited an absorption peak at 820 nm when dispersed in water, as shown in Figure 2a, which is in agreement with a previous report.[13] The gold nanorods were successfully trapped in a matrix of pNIPAAm particles, which was confirmed by TEM analysis, as shown in Figure 2b, where a dried gel particle with a diameter of 750 nm can be seen. Figure 2c shows the temperature dependence of the volume of the hydrogel particle, where the volume is measured after incubation for 10 min at each temperature. The copolymerization of METAC with NIPAAm increases the transition temperature and makes the transition significantly broader.[17] A dramatic change in volume was observed around 45 °C, which is much higher than the LCST of pure pNIPAAm at 32°C.

To confirm the light-triggered volume change of the hydrogel particles, we prepared an ethyl cellulose film containing gold nanorod-embedded pNIPAAm particles, where organic solution, same as the middle oil phase used for double-emulsion formation, was deposited on the glass substrate and consolidated. After complete evaporation of volatile solvents, the ethyl cellulose film on the glass substrate was immersed in water, and a size change of the pNIPAAm particles was seen. For clear observation of this change in size, hydrogel particles with a diameter of approximately 200 μm were used in this case. The NIR light source consisted of a laser with a power of 1 W and a wavelength of 808 nm, which is close to the plasmon band of gold nanorods. On NIR light exposure for 15 s, the hydrogel particles containing the gold nanorods shrank to approximately 65% of their original volumes. In addition, the particles recovered to almost their

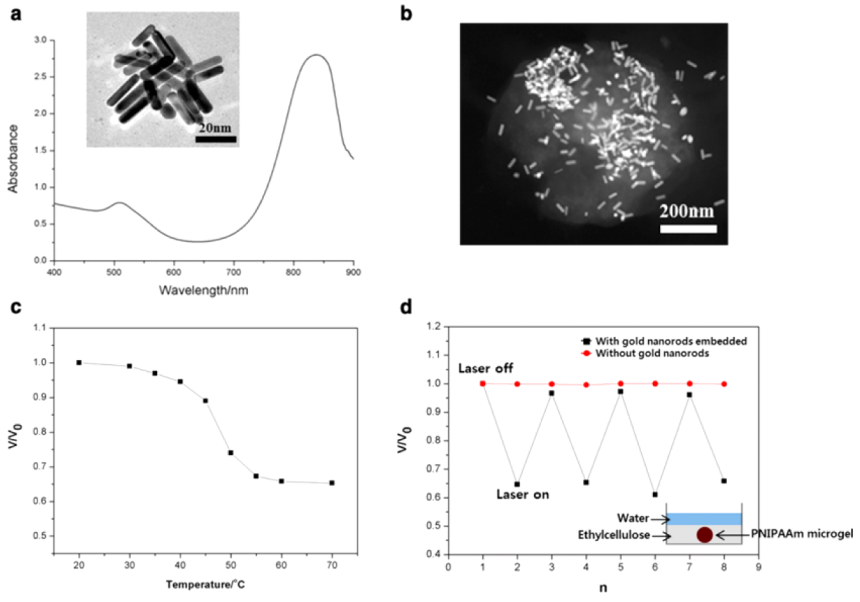

Figure 2. (a) Absorption spectrum of the gold nanorods dispersed in water. Inset shows a TEM image of the gold nanorods. (b) TEM image of pNIPAAm hydrogel particle containing gold nanorods. (c) Temperature dependence of the volume of the hydrogel particle, where the volume is normalized with volume at 20 °C. (d) Volume change of gold nanorod-embedded pNIPAAm particle (black squares) in the matrix of ethyl cellulose according to a cycle of laser on and off, where the volume is normalized to the initial volume, V_0. For comparison, pNIPAAm particles without gold nanorods were also used (red dots).

dx.doi.org/10.1021/am4037993 | ACS Appl. Mater. Interfaces 2014, 6, 826−832

original volume in just 30 s after the laser was turned off. This volume transition was found to be highly reversible, as can be seen from the black squares in Figure 2d, where the change in volume (V/V_0) was plotted as a function of the cycle number of laser on−off events. The cycle was repeated more than 8 times, with variation between each swollen state or each deswollen state being less than 3.4%. The dynamic volume change can also be clearly seen in Movie S1 of the Supporting Information. In contrast, the same particles without gold nanorods remained unchanged, regardless of laser irradiation, as shown by the red dots in Figure 2d. This demonstrates that the absorption of light by the gold nanorods increased the temperature of the pNIPAAm particles above the LCST.

To produce microcapsules composed of an aqueous core and pNIPAAm particle-embedded ethyl cellulose shell, double-emulsion drops were employed as templates. Monodisperse double-emulsion drops were prepared using a microfluidic device that was simply assembled from pipette tips and a glass capillary, as shown in Figure 3a and Figures S1 and S2 of the Supporting Information. An aqueous solution of 2 wt % PVA and 2 wt % FITC-dextran as a model drug was used to form the innermost drops and was injected through the smallest pipette tip. A mixture of DCM and hexane containing 8 wt % ethyl cellulose and the pNIPAAm particles was used to form the outer drops and was injected through the interstices between the smallest and the second pipette tips. The hydrophobic nature of the tips promoted wetting of the middle oil phase on the inner surface of the second tip and the outer surface of the smallest tip, while preventing wetting of the aqueous solution on the outer surface of the smallest tip. The aqueous solution of 2 wt % PVA was also used to form the continuous phase and was injected through the interstices between the glass capillary and the third pipette tip. The hydrophilic nature of glass prevented wetting of the oil phase on the inner surface of the glass capillary. All three phases were coaxially injected through the orifice of the glass capillary, and double-emulsion drops were formed by single-step emulsification. A break in the inner interface between the innermost aqueous and middle oil phases occurred immediately before a break in the outer interface between the middle oil and continuous aqueous phases. Typically, the device was operated at volumetric flow rates of the innermost, middle, and continuous fluids of 0.15, 0.35, and 3 mL/h, respectively. Double-emulsion formation at these flow rates is shown in Figure 3b and Movie S2 in the Supporting Information. The flow rate of the continuous phase was further adjusted to control the size of the double-emulsion drops. As the flow rate was increased from 3 to 12 mL/h, the diameter of the double-emulsion droplets decreased from 530 to 280 μm, as shown in Figure 3c. This was due to a higher drag force being exerted on the hanging droplets at the junction, owing to the higher flow rate of the continuous phase. The prepared double-emulsion drops were collected in an aqueous solution of 0.5 wt % PVA, as shown in Figure 3d. The drops were then incubated in an open chamber to evaporate the organic solvents from the oil shell, transforming into opaque microcapsules after the consolidation was fully completed (inset, Figure 3d). During the evaporation process, the inner drop remained unchanged, and the middle oil phase became a thinner solid shell that encapsulated the inner drop. The shell membrane, doped with Nile Red, can be clearly observed in the fluorescence microscopy image shown in Figure 3e, with the average thickness of the shell measured to be approximately 15 μm. In addition, the aqueous core containing the FITC-dextran can also be seen (inset, Figure 3e).

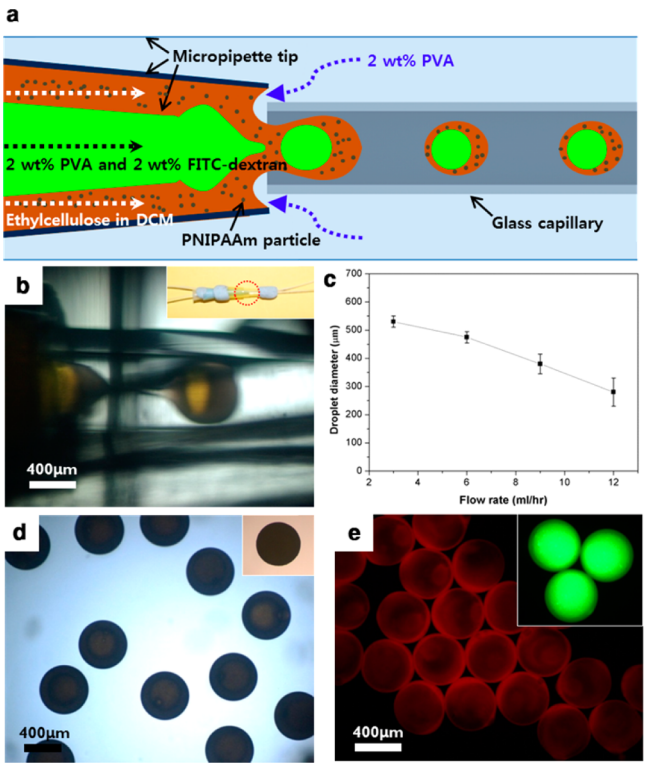

Figure 3. (a) Schematic illustration of the microfluidic device used for preparation of the double-emulsion drops. (b) Optical microscope image showing generation of the double-emulsion drops by single-step emulsification (see also Movie S2 of the Supporting Information). (c) Influence of flow rate of the continuous phase on the diameter of double-emulsion drops, where the flow rates for the inner and middle fluids were kept at 0.15 and 0.3 mL/h, respectively. The error bar represents the standard deviation. (d) Optical microscope image of monodisperse double-emulsion drops. Inset shows a microcapsule after consolidation is complete. (e) Fluorescence microscope image of microcapsules containing Nile Red. Inset shows microcapsules whose aqueous core contains FITC-dextran.

We examined the surface morphology of the dried microcapsules using SEM, as shown in Figure 4. Both surface and internal pores are observed, which would be partially occupied by pNIPAAm particles in the low-temperature swollen state. During the drying process required for SEM observation, the pNIPAAm particles would collapse, leaving the pores. The size of pores was in the range of submicrometer to a few micrometers, which is consistent with the size of the pNIPAAm particles in the middle oil phase, as shown in Figure S3 (Supporting Information). We also prepared the microcapsules without pNIPAAm particles to compare pores in the membrane. As shown in Figure S4 of the Supporting Information, the microcapsules have internal pores at lower density, which result from the fast evaporation of organic solvents,[18,19] and very low density of surface pores. Therefore, part of the internal pores in the dried microcapsules with pNIPAAm particles is formed not by the pNIPAAm particles but by the fast evaporation of solvent. In the cross-section image in Figure 4d, highly porous and interconnected morphology is shown, which proves that pNIPAAm particles in the swollen state can act as valves for diffusion of encapsulants through the membrane.[20,21]

dx.doi.org/10.1021/am4037993 | ACS Appl. Mater. Interfaces 2014, 6, 826−832

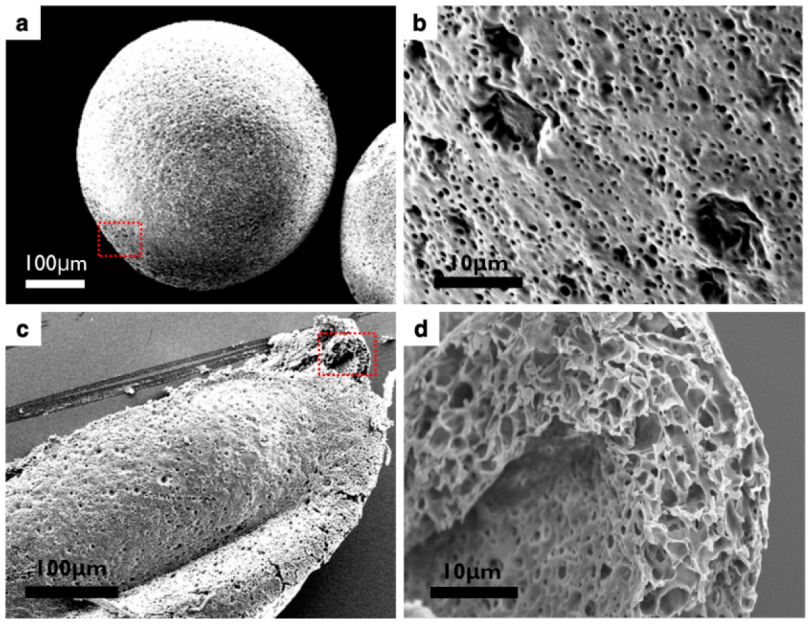

Figure 4. SEM images of a dried microcapsule showing (a, b) surface and (c, d) cross-section of the membrane. To enable observation of the shell cross sections, the microcapsules were cut using a razor blade. Polydisperse pores are densely packed and interconnected.

To confirm the thermoresponsiveness of the system, the release profile of FITC-labeled dextran molecules from the microcapsules was evaluated at 25 °C and 55 °C (Figure 5a).

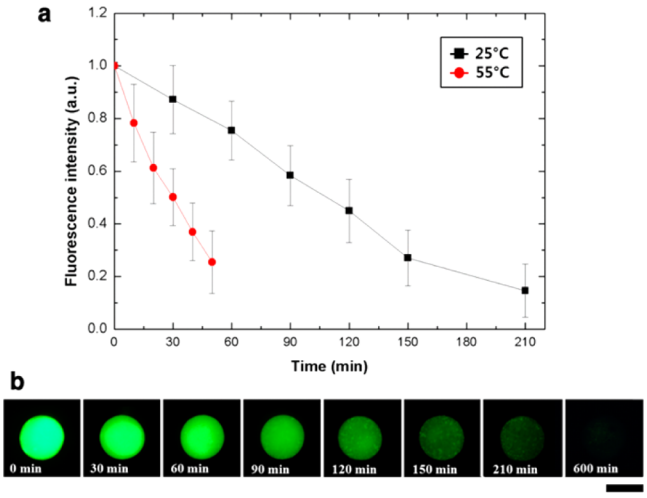

Figure 5. (a) Time dependence of fluorescence intensity inside the microcapsules, where the microcapsules were incubated at two different temperatures of 25 °C (black squares) and 55 °C (red dots). These intensity profiles were obtained from 25 microcapsules per data point. The error bar represents the standard deviation. (b) A series of fluorescence microscope images of the microcapsule incubated at 25 °C; scale bar is 400 μm.

The fluorescence intensity of the microcapsules was calculated from the fluorescence microscopy images shown in Figure 5b. It can be seen that the dextran slowly leaked through the membrane, even at 25 °C, which is below the LCST of the pNIPAAm; however, it took 150 min for the fluorescence of the dextran to reach 27% of the original intensity. This slow leakage was attributed to the large mesh size of the pNIPAAm hydrogel. In contrast, the release was found to be 3-fold faster at a temperature of 55 °C, with only 50 min required to reach the same reduced fluorescence intensity. This demonstrated the higher permeability of the membrane at the temperature above the LCST. At the higher temperature, all the pNIPAAm particles would be fully collapsed, leaving macrogaps between the particles and the ethyl cellulose shell matrix. These macrogaps would provide a pathway through which the FITC-dextran would be able to diffuse, resulting in its rapid release. The permeability of the shell could potentially be further tuned by adjusting the density of hydrogel particles, the shell wall thickness, and the capsule size. In the microcapsules without pNIPAAm particles as shown in Figure S4 (Supporting Information), insignificant leakage of FITC-labeled dextran was observed in the experimental time scale of 210 min due to lack of pore interconnectivity.

The photoresponsiveness of the microcapsules was evaluated by measuring the fluorescence intensity outside the microcapsules incubated at 25 °C. The surrounding fluid was then refreshed 10 min before NIR laser exposure to remove any released dextran. The difference in fluorescence intensity immediately before and after laser exposure for 30 s was measured. This exposure was carried out repeatedly at intervals of 30 min. The fluorescence intensities and microscopy images are summarized in Figures 6a and b, respectively. Before the first exposure to the NIR laser, the fluorescence intensity outside the microcapsules was consistently low, as can be seen in the first image in the top row. Upon laser exposure, the dextran was abruptly released, as shown in the first image of the bottom row, resulting in a 4-fold increase in fluorescence intensity. This release was caused by the photothermal effect of the gold nanorods on absorption of the NIR radiation. When the laser was turned off, the hydrogel particles would cool down and then swell, thereby refilling the pores. This was demonstrated by the rate of flux of dextran out of the capsules returning to the pre-irradiation level. The same trends were observed for each of the subsequent repetitive laser exposures; however, the quantity of released dextran gradually decreased at each exposure as the concentration of FITC-dextran inside the microcapsules decreased. The release upon laser irradiation

dx.doi.org/10.1021/am4037993 | ACS Appl. Mater. Interfaces 2014, 6, 826−832

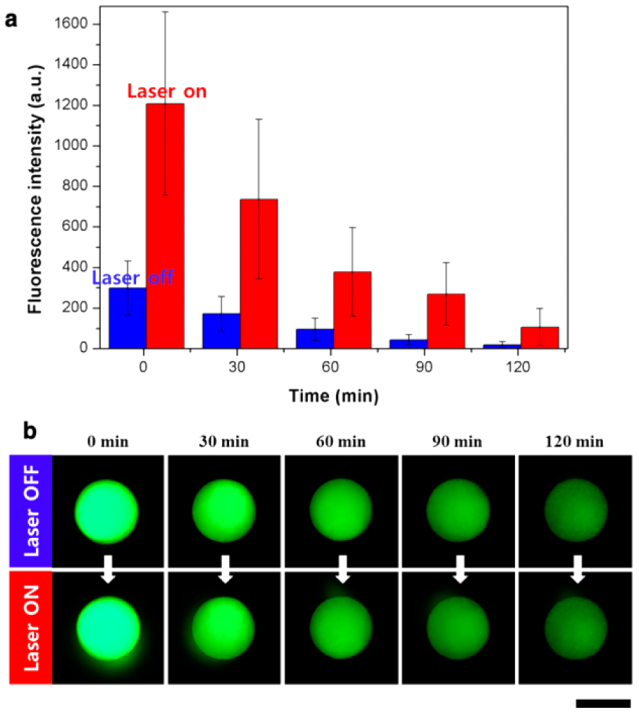

Figure 6. (a) Fluorescence intensity outside the microcapsule before (blue) and after (red) irradiation with NIR laser for 30 s, where the capsules were repeatedly exposed at intervals of 30 min. Average fluorescence intensities were calculated from 25 microcapsules. The error bar represents the standard deviation. (b) Corresponding fluorescence microscope images of the microcapsule taken at the denoted times before (top row) and after (bottom row) laser irradiation (see also Movie S3 of Supporting Information). Microcapsules were incubated at 25 °C; scale bar is 400 μm.

occurs anisotropically as shown in Figure 6b. We attribute this one-sided release rather than isotropic release to high polydispersity of the hydrogel particles and their uneven distribution within the membrane. For the same reasons, there exists a large standard deviation in the fluorescence intensity as shown in Figure 6a; the average and standard deviation were calculated from 25 microcapsules randomly selected. This capsule-to-capsule variation could potentially be reduced by making more uniform hydrogel particles through improved microfluidics or by using membrane emulsification rather than bulk emulsification.[22,23] In the control experiment, where there were no gold nanorods in the pNIPAAm particles, no increase in fluorescence intensity was observed on NIR irradiation, providing further evidence of the local heating effect of these structures.

CONCLUSIONS

We have developed NIR light-sensitive, mechanically stable microcapsules that can undergo reversible permeability changes for controlled release of an encapsulant. W/O/W double-emulsion drops were prepared using a simple and cheap microfluidic device and were used as templates for the microcapsules. The middle oil phase was carefully selected to produce the photoresponsive membrane of the microcapsules, and the ethyl cellulose membrane was designed to contain a dense packing of gold nanorod-embedded pNIPAAm particles. The gold nanorods absorbed NIR light and increased the temperature of the hydrogel particles, which then shrank when above the LCST of the polymer. This resulted in the formation of macrogaps between the particles and shell matrix, through which relatively large molecules could pass. This combination of structures enabled the remote control of membrane permeability by NIR light. The open and closed states of hydrogel valves could be reversibly switched, allowing programmed release of encapsulants. In addition, the resultant microcapsules had high mechanical stability and, owing to the polymers used, would be biocompatible. Moreover, pNIPAAm microgels embedded in the membrane can exhibit phase transition in response to a temperature or light stimuli, when subjected to the common physiological conditions of ion concentration and pH. Therefore, the developed microcapsules and proposed valve actuation in the membrane have great potential for on-demand in vivo release, especially for implantation-based delivery of drugs with high molecular weights.

ASSOCIATED CONTENT

Supporting Information

Images showing the fabrication procedure of the fluidic device and optical microscopy images showing the middle oil phase are included. In addition, Movies S1−3 show the light-induced volume change of the hydrogel particles, generation of the double-emulsion drops, and light-triggered release of encapsulants. This material is available free of charge via the Internet at http://pubs.acs.org.

AUTHOR INFORMATION

Corresponding Authors

*E-mail: kim.sh@kaist.ac.kr (S.-H.K.).
*E-mail: smyang@kaist.ac.kr (S.-M.Y.)

Notes

The authors declare no competing financial interest.

ACKNOWLEDGMENTS

This work was supported by a grant from the Creative Research Initiative Program of the Ministry of Science, ICT, and Future Planning for "Complementary Hybridization of Optical and Fluidic Devices for Integrated Optofluidic Systems". This research was also supported by a WCU (World Class University) program through a National Research Foundation of Korea (NRF) grant funded by the Korean government (MSIP) (No. 2006-0050630). The authors also appreciate partial support from the BK21 Plus Program.

DEDICATION

[§]Professor Yang passed away unexpectedly on September 26, 2013. We dedicate this work as a memorial to him.

REFERENCES

(1) Bawa, P.; Pillay, V.; Choonara, Y. E.; du Toit, L. C. *Biomed. Mater.* **2009**, *4*, 022001.
(2) Hoare, T.; Timko, B. P.; Santamaria, J.; Goya, G. F.; Irusta, S.; Lau, S.; Stefanescu, C. F.; Lin, D.; Langer, R.; Kohane, D. S. *Nano Lett.* **2011**, *11*, 1395−1400.
(3) Jeon, G.; Yang, S. Y.; Byun, J.; Kim, J. K. *Nano Lett.* **2011**, *11*, 1284−1288.
(4) Pastine, S. J.; Okawa, D.; Zettl, A.; Fréchet, J. M. *J. Am. Chem. Soc.* **2009**, *131*, 13586−13587.
(5) Hribar, K. C.; Lee, M. H.; Lee, D.; Burdick, J. A. *ACS Nano* **2011**, *5*, 2948−2956.
(6) Skirtach, A. G.; Karageorgiev, P.; Bédard, M. F.; Sukhorukov, G. B.; Möhwald, H. *J. Am. Chem. Soc.* **2008**, *130*, 11572−11573.

(7) Lee, M. H.; Hribar, K. C.; Brugarolas, T.; Kamat, N. P.; Burdick, J. A.; Lee, D. *Adv. Funct. Mater.* **2012**, *22*, 131−138.
(8) Amstad, E.; Kim, S. H.; Weitz, D. A. *Angew. Chem.* **2012**, *124*, 12667−12671.
(9) Kim, B.; Lee, H. S.; Kim, J.; Kim, S.-H. *Chem. Commun.* **2013**, *49*, 1865−1867.
(10) Seiffert, S.; Weitz, D. A. *Soft Matter* **2010**, *6*, 3184−3190.
(11) Shibayama, M. *Bull. Chem. Soc. Jpn.* **2006**, *79*, 1799−1819.
(12) Shiotani, A.; Mori, T.; Niidome, T.; Niidome, Y.; Katayama, Y. *Langmuir* **2007**, *23*, 4012−4018.
(13) Nikoobakht, B.; El-Sayed, M. A. *Chem. Mater.* **2003**, *15*, 1957−1962.
(14) Murtaza, G. *Acta Pol. Pharm. Drug Res.* **2012**, *69*, 11−22.
(15) Ahmad, M.; Madni, A.; Usman, M.; Munir, A.; Akhtar, N.; Khan, H. M. S. *World Acad. Sci., Eng. Technol.* **2011**, *51*, 384−387.
(16) Yue, L.-L.; Xie, R.; Wei, J.; Ju, X.-J.; Wang, W.; Chu, L.-Y. *J. Colloid Interface Sci.* **2012**, *377*, 137−144.
(17) Mun, G. A.; Nurkeeva, Z. S.; Khutoryanskiy, V. V.; Sergaziyev, A. D.; Rosiak, J. M. *Radiat. Phys. Chem.* **2002**, *65*, 67−70.
(18) Liu, L.; Yang, J.-P.; Ju, X.-J.; Xie, R.; Yang, L.; Liang, B.; Chu, L.-Y. *J. Colloid Interface Sci.* **2009**, *336*, 100−106.
(19) Yu, Y.-L.; Zhang, M.-J.; Xie, R.; Ju, X.-J.; Wang, J.-Y.; Pi, S.-W.; Chu, L.-Y. *J. Colloid Interface Sci.* **2012**, *376*, 97−106.
(20) Moura, M. R. d.; Guilherme, M. R.; Campese, G. M.; Radovanovic, E.; Rubira, A. F.; Muniz, E.C. *Eur. Polym. J.* **2005**, *41*, 2845−2852.
(21) Wang, J.; Zhou, X.; Xiao, H. *Carbohydr. Polym.* **2013**, *94*, 749−754.
(22) Jeong, W.-C.; Lim, J.-M.; Choi, J.-H.; Kim, J.-H.; Lee, Y.-J.; Kim, S.-H.; Lee, G.; Kim, J.-D.; Yi, G.-R.; Yang, S.-M. *Lab Chip* **2012**, *12*, 1446−1453.
(23) Wang, Y.; Qin, J.; Wei, Y.; Li, C.; Ma, G. *Powder Technol.* **2013**, *236*, 107−113.